

Dynamics of a nanowire superlattice in an ac electric field

Aizhen Zhang and L. C. Lew Yan Voon*

*Department of Physics, Wright State University,
3640 Colonel Glenn Highway, Dayton, Ohio 45435, USA*

M. Willatzen

*Mads Clausen Institute, University of Southern Denmark,
Grundtvigs Allé 150, DK-6400 Sønderborg, Denmark*

(Dated: September 12, 2018)

Abstract

With a one-band envelope function theory, we investigate the dynamics of a finite nanowire superlattice driven by an ac electric field by solving numerically the time-dependent Schrödinger equation. We find that for an ac electric field resonant with two energy levels located in two different minibands, the coherent dynamics in nanowire superlattices is much more complex as compared to the standard two-level description. Depending on the energy levels involved in the transitions, the coherent oscillations exhibit different patterns. A signature of barrier-well inversion phenomenon in nanowire superlattices is also obtained.

I. INTRODUCTION

Semiconductor quantum dots (QDs), also called “artificial atoms,” are being considered for a variety of technological applications ranging from semiconductor electronics to biological applications including optical devices, quantum computing and biosensors. The study of coherent phenomena is fundamental to a wide range of these applications. For example, a large number of experimental and theoretical investigations of Rabi oscillations (ROs), the analog of atom-light coherent nonlinear interactions, have been performed in the quantum-dot two-level systems in single QDs^{1,2,3,4,5,6,7,8,9,10} and double QDs.^{11,12}

If we deal with an array of QDs, the discrete levels broaden into energy bands. The question then arises whether coherent oscillations can be observed in such structures. The formation of minibands with discrete states for a system of fifteen coupled QDs in a matrix has been demonstrated.¹³ Quantum transport in a model one-dimensional quantum dot array under a dc bias has also been studied theoretically.¹⁴ Another different type of QD array, so-called nanowire superlattices (NWSLs),^{15,16,17,18,19} has recently been fabricated using various approaches. A nanowire superlattice consists of a series of interlaced nanodots of two different materials. In NWSLs, the electronic transport along the wire axis is made possible by the tunneling between adjacent dots, while the uniqueness of each quantum dot and its zero-dimensional (0D) characteristics are maintained by the energy difference of the conduction or valence bands between the different materials. The band offset not only provides some amount of quantum confinement, but also creates a periodic potential for carriers moving along the wire axis. This new structure offers unique features and suggests a diversity of possible applications, including nanolasers, nanobarcodes, one-dimensional (1D) waveguides, resonant tunneling diodes, and thermoelectrics.

The successful experimental developments of NWSLs have received increasing theoretical attention. Recently considerable work has been devoted to NWSLs.^{20,21,22,23,24,25,26} Lew Yan Voon and Willatzen²⁰ have first studied the electron states and optical properties in NWSLs. The thermoelectric properties of NWSLs have been reported by Lin and Dresselhaus.²³ Citrin²⁴ has investigated the magnetic Bloch oscillations in nanowire superlattice rings. Madureira *et al.*²⁵ have proposed that dynamic localization should be observable in NWSLs. A detailed study of acoustic phonons in NWSLs has been given by Mizuno.²⁶

With the development of free-electron lasers that can be continuously tuned in the tera-

hertz (THz) range, the dynamics of charged particles in semiconductor nanostructures has been a subject of intensive research. Motivated by the experimental progress and the importance to many applications of NWSLs, in this work, we study the dynamics of a NWSL driven by an ac electric field as a realistic system of a finite chain of coupled QDs. Diez *et al.*²⁷ have investigated the dynamics of a finite semiconductor quantum well superlattice (SL) in an ac electric field and found that Rabi oscillations between minibands are clearly identified under resonant conditions. However, our system is different from SLs in a number of aspects. The coupling of the superlattice longitudinal confinement to nanowire radial confinement in NWSL leads to an additional position-dependent potential for the electron. Furthermore, for a nanowire superlattice, using a position-dependent effective mass leads to qualitatively new physics.²⁰ Given these unique features, we expect that the dynamics of NWSLs driven by an ac electric field would reveal more interesting results.

The paper is organized as follows. In Sec. II we introduce the model and present the theory. In Sec. III, we present the numerical results. A summary is given in Section IV.

II. THEORY

In this section we present the theoretical model and approach. The model is essentially the same as the one used in Ref. 20. We briefly describe the model for completeness. The finite NWSL is modeled as an ideal cylinder surrounded by vacuum with sharp modulations in the longitudinal (or z) direction (Fig. 1). The electronic structure is obtained by solving the BenDaniel-Duke equation

$$-\frac{\hbar^2}{2}\nabla\cdot\left[\frac{1}{m(\mathbf{r})}\nabla\psi(\mathbf{r})\right]+V(\mathbf{r})\psi(\mathbf{r})=E\psi(\mathbf{r}), \quad (1)$$

where $V(\mathbf{r})$ is the potential experienced by the electron, $m(\mathbf{r})$ is the effective mass in each layer, $\psi(\mathbf{r})$ is the wave function, and E is the energy. This model is appropriate for conduction states and for large band-gap materials when nonparabolicity can be neglected. This partial differential equation is separable in cylindrical circular coordinates, leading to the following set of ordinary differential equations,

$$\frac{d^2\Phi(\phi)}{d\phi^2}+l^2\Phi(\phi)=0, \quad (2)$$

$$r\frac{d}{dr}\left(r\frac{dJ}{dr}\right)+\left(q^2r^2-l^2\right)J(r)=0, \quad (3)$$

$$-\frac{\hbar^2}{2} \frac{d}{dz} \left(\frac{1}{m(z)} \frac{dZ(z)}{dz} \right) + \left[V(z) + \frac{\hbar^2 q^2}{2m(z)} \right] Z(z) = EZ(z), \quad (4)$$

where $\psi(\mathbf{r}, \phi, z) = J(r)\Phi(\phi)Z(z)$.

The solution to the angular Eq. (2) is $\Phi(\phi) = e^{il\phi}$ with l an integer. The solution to the radial Eq. (3) is a Bessel function of the first kind, with the wavenumber q determined by the boundary condition $J_l(qR) = 0$, where R is the radius of the NWSL. Because the zeros of the Bessel functions are themselves independent of the structure, we only have to solve the longitudinal Eq. (4). Equation (4) describes an electron moving in a one-dimensional effective potential $V^{eff}(z) = V(z) + \frac{\hbar^2 q^2}{2m(z)}$. For typical semiconductors, the well mass m_W is smaller than the barrier mass m_B . Thus the effective potential can be zero or negative if

$$R^2 \leq \frac{\hbar^2 \alpha^2 [m_B(z) - m_W(z)]}{2V_B(z) m_W(z) m_B(z)} = R_c^2, \quad (5)$$

where $V_B(z)$ is the real barrier height and α is a zero of the Bessel function. Hence, below a critical radius R_c , the barrier layer acts as the well layer and vice versa. The barrier-well inversion induced by quantum confinement, a unique phenomenon in NWSLs, was predicted in Ref. 20.

In order to study the dynamics of the NWSL driven by an ac electric field, we must determine the band structure. At flatband, the band structure of Eq. (4) is computed by using the finite-element method. The eigenstate j of band i with eigenenergy $E_i^{(j)}$ is denoted as $Z_i^{(j)}(z)$. Under an ac electric field, the envelope function for the electron wave packet satisfies the following equation

$$i\hbar \frac{d}{dt} \Psi(z, t) = \left\{ -\frac{\hbar^2}{2} \frac{d}{dz} \left(\frac{1}{m(z)} \frac{d}{dz} \right) + \left[V(z) + \frac{\hbar^2 q^2}{2m(z)} \right] - eFz \sin(\omega_{ac}t) \right\} \Psi(z, t), \quad (6)$$

where F and ω_{ac} are the strength and the frequency of the ac field. Given the form of the initial wave function $\Psi(z, 0)$, the time-dependent Schrödinger Eq. (6) is solved using the finite-difference method and a fourth order Runge-Kutta integration. The mesh spacing is 0.1 nm and the time step is of the order 10^{-6} ps, which ensure the accuracy of the numerical calculation. For the sake of simplicity, we have selected $\Psi(z, 0) = Z_i^{(j)}(z)$ as the initial wave packet. The probability of finding the electron in the state $Z_k^{(l)}(z)$ is given by

$$P_{ik}^{(jl)} = \left| \int_{-\infty}^{+\infty} dz Z_k^{(l)}(z) \Psi(z, t) \right|^2. \quad (7)$$

Note that, for the case of a two-level system with levels a and b driven by a strong resonant field, the driving field couples levels a and b and induces oscillations of the population in

the two levels, the so-called Rabi oscillations. The frequency Ω_R of the ROs is proportional to the electric field amplitude and the dipole transition matrix element, which is given by

$$\Omega_R = eF_{Thz} \langle \psi_a | x | \psi_b \rangle / \hbar = eF_{Thz} x_{ab} / \hbar, \quad (8)$$

where F_{Thz} is the amplitude of the terahertz electric field, $|\psi_a\rangle$ and $|\psi_b\rangle$ are respectively the unperturbed eigenfunctions of levels a and b , and ex_{ab} is the dipole transition matrix element with e the electric charge. If the particle is initially in level a , the probability of finding the electron in level b oscillates between 0 and 1, i.e, complete resonance occurs.

III. RESULTS

We consider a GaAs/GaAlAs NWSL structure with 10 periods of 5 nm GaAlAs and 9 periods of 10 nm GaAs terminated by a cylindrical 100 nm GaAs layer on each side (Fig. 1). Such a structure can be well described by Eq. (1). In the calculation we use parameters $\alpha = 2.405$ (the first root of zeroth order Bessel function), $V_z = 230$ meV, $m_B(z) = 0.0919m_0$, and $m_W(z) = 0.067m_0$, where m_0 is the free-electron mass. The resulting critical radius $R_c = 2$ nm for such a structure. We first choose $R = 5$ nm, which is larger than the critical radius. We begin by considering the case of resonant excitation with $F = 50$ kV/cm. Figure 2(a) shows $P_{12}^{(55)}(t)$ at the resonant frequency $\omega_{ac} = (E_2^{(5)} - E_1^{(5)}) / \hbar = 127$ THz, i.e., we are monitoring the transition between the central state $j = 5$ in the first miniband to the central state $l = 5$ in the second miniband. As can be seen, the oscillations reveal the occurrence of coherent oscillations between minibands. This is qualitatively similar to the picture reported for one-dimensional superlattices.²⁷ Figure 2(b) displays $P_{12}^{(22)}(t)$ at the resonant frequency $\omega_{ac} = (E_2^{(2)} - E_1^{(2)}) / \hbar = 121$ THz, i.e, the transitions between the second state $j = 2$ in the first miniband to the second state $l = 2$ in the second miniband. There are two main differences in the oscillations in comparison to Fig. 2(a). Firstly, the oscillation peak values are smaller. Secondly, the oscillations have a decreasing amplitude tendency. This is due to the higher probability of the electron tunnelling to the outer GaAs layers when the energy levels are close to the boundary of the actual structure, because in the calculation we have considered an overall structure much larger than the actual NWSL region. In Fig. 2(c) we present $P_{12}^{(56)}(t)$ at the resonant frequency $\omega_{ac} = (E_2^{(6)} - E_1^{(5)}) / \hbar = 131$ THz, i.e., the probability of finding the electron, initially in the central state $j = 5$ in the first miniband, in

the state $l = 6$ in the second miniband at time t . We find that coherent oscillations between minibands can also be clearly identified except that the peak values are smaller than in Fig. 2(a). By performing the fast Fourier transform of $P_{12}^{(55)}(t)$, $P_{12}^{(22)}(t)$, and $P_{12}^{(56)}(t)$, we find that the oscillation frequencies are 15.1 THz, 19.1 THz, and 16.0 THz, respectively.

The different oscillation patterns and oscillation frequencies shown in Fig. 2 can be understood as follows. The considered nanowire superlattice structure presents Bloch minibands with nine states in each miniband. These states are closely spaced with separations less than 1 meV. When a resonant ac electric field is applied to two energy levels respectively located in the first miniband and the second miniband, a number of energy levels are involved in the transitions. As a result, the probability of finding the electron in the energy level in the second miniband is much less than 1 (as shown in Fig. 2). To further check the validity of the two-level description, we calculate the oscillation frequencies corresponding to the three cases shown in Fig. 2 using the analytic Eq. (8) of a driven two-level system. The resulting frequencies are 19 THz, 4.9×10^{-2} THz, and 2.1×10^{-2} THz, respectively, which, except for the first one, are very different from the values obtained by performing the fast Fourier transform of $P_{12}^{(55)}(t)$, $P_{12}^{(22)}(t)$, and $P_{12}^{(56)}(t)$. Thus it is clear that the two-state description is not generally valid for a NWSL. In the three cases shown in Fig. 2, different energy levels and therefore different eigenfunctions are involved in the transitions, leading to different oscillation patterns and oscillation frequencies. Although the occurrence of ROs has been identified in Ref. 27, the important features of the sensitivity of ROs to the energy levels involved in the transitions and the inapplicability of two-level theory were not pointed out. Furthermore, because the electron can be driven up to the third miniband, we find that the total probability of finding the electron in the second miniband cannot reach 1 maximally.

We now turn to the case of nonresonant excitation. Figures 3(a)–3(c) show the transition probability $P_{12}^{(55)}(t)$, $P_{12}^{(22)}(t)$, and $P_{12}^{(56)}(t)$ with $\omega_{ac} = 100$ THz and $F = 50$ kV/cm respectively. In contrast to the resonant situation, one can see that the oscillation amplitudes are significantly decreased in all three cases when the ac driving field is out of resonance.

Next we discuss the barrier-well inversion induced by quantum confinement predicted in Ref. 20. When $R < R_c$, the barrier becomes the well and vice versa. For the GaAs/GaAlAs NWSL structure discussed here, the barrier width increases if the barrier-well inversion occurs, resulting in a narrower band width and a larger band gap. The energy levels in the minibands become more closely spaced and the wavefunctions change dramatically. To

compare with the case of $R > R_c$, in Fig. 4 we show the calculated $P_{12}^{(55)}(t)$ with $R = 1$ nm (less than critical radius). Other parameters are the same as used in Fig. 2(a). As expected, the oscillation pattern is totally different from Fig. 2(a) due to different band structures. Both the amplitudes and the frequency are found to be greatly decreased. Therefore the barrier-well inversion phenomenon is verified by the transport properties presented here.

IV. SUMMARY

In this paper, within a one-band envelope function theory and by means of numerically solving the time-dependent Schrödinger equation, we have presented an analysis of the dynamics of a finite NWSL driven by an ac electric field. We have found that for the case of resonant ac electric field, the coherent dynamics is much more complex as compared to the standard two-level description. The oscillations are extremely sensitive to the energy levels involved in the transitions. As a result, the oscillation patterns are very different when the applied ac electric field is resonant with two different energy levels respectively located in the first and second minibands. Coherent oscillations between minibands can be identified when the probability of the tunneling of the electron to the surrounding region is negligible. On the other hand, the oscillations can also exhibit a decreasing amplitude tendency due to the greater probability of the electron tunneling to the surrounding region. In comparison to the resonant case, the oscillation amplitudes are significantly decreased when the ac electric field is out of resonance. We have also verified the existence of barrier-well inversion phenomena due to the coupling of the superlattice longitudinal confinement to nanowire radial confinement in NWSLs. This indicates that the radius of NWSL should be kept in mind for investigating a variety of phenomena.

Nanowire superlattices do have some advantages over other nanostructures: (i) scattering events are highly suppressed because of the spatial confinement of carriers along all three directions, leading to a long decoherence time, (ii) the wire structure lacks the transverse excitations present in quantum-well superlattice structures, eliminating this source of damping, and (iii) this novel structure has no wetting layer (WL) compared with previously-studied single and double QDs. These make NWSLs potentially more favorable for observations of coherent phenomena. However, due to the structural complexity and the materials diversity in these nanostructures, for practical applications and device optimization it is essential to

develop appropriate models to understand the behavior and to predict properties of interest in these novel structures. Work along these lines is currently in progress.

Acknowledgments

The work was supported by an NSF CAREER award (NSF Grant No. 0454849), and by a Research Challenge grant from Wright State University and the Ohio Board of Regents.

-
- * Electronic address: lok.lewyanvoon@wright.edu
- ¹ T. H. Stievater, X. Li, D. G. Steel, D. Gammon, D. S. Katzer, D. Park, C. Piermarocchi, and L. J. Sham, *Phys. Rev. Lett.* **87**, 133603 (2001).
 - ² H. Kamada, H. Gotoh, J. Temmyo, T. Takagahara, and H. Ando, *Phys. Rev. Lett.* **87**, 246401 (2001).
 - ³ H. Htoon, T. Takagahara, D. Kulik, O. Baklenov, A. L. Holmes, Jr., and C. K. Shih, *Phys. Rev. Lett.* **88**, 087401 (2002).
 - ⁴ A. Zrenner, E. Eham, S. Stuffer, F. Findeis, M. Bichler, and G. Abstreiter, *Nature (London)* **418**, 612 (2002).
 - ⁵ P. Borri, W. Langbein, S. Schneider, U. Woggon, R. L. Sellin, D. Ouyang, and D. Bimberg, *Phys. Rev. B* **66**, 081306(R) (2002).
 - ⁶ L. Besombes, J.J. Baumberg, and J. Motohisa, *Phys. Rev. Lett.* **90**, 257402 (2003).
 - ⁷ A. Muller, Q.Q. Wang, P. Biancci, C.K. Shih, and Q. K. Cue, *Appl. Phys. Lett.* **84**, 981 (2004).
 - ⁸ Q. Q. Wang, A. Muller, P. Bianucci, E. Rossi, Q. K. Xue, T. Takagahara, C. Piermarocchi, A. H. MacDonald, and C. K. Shih, *Phys. Rev. B* **72**, 035306 (2005).
 - ⁹ X. Li, Y. Wu, D. Steel, D. Gammon, T.H. Stievater, D.S. Katzer, D. Park, C. Piermarocchi, and L.J. Sham, *Science* **301**, 809 (2003).
 - ¹⁰ J. M. Villas-Bôas, Sergio E. Ulloa, and A. O. Govorov, *Phys. Rev. Lett.* **94**, 057404 (2005).
 - ¹¹ T. Hayashi, T. Fujisawa, H. D. Cheong, Y. H. Jeong, and Y. Hirayama, *Phys. Rev. Lett.* **91**, 226804 (2003).
 - ¹² J. R. Petta, A. C. Johnson, C. M. Marcus, M. P. Hanson, and A.C. Gossard, *Phys. Rev. Lett.* **93**, 186802 (2004).
 - ¹³ L. P. Kouwenhoven, F. W. J. Hekking, B. J. van Wees, C. J. P. M. Harmans, C. E. Timmering, and C. T. Foxon, *Phys. Rev. Lett.* **65**, 361 (1990).
 - ¹⁴ W. Z. Shangguan, T. C. Au Yeung, Y. B. Yu, and C. H. Kam, *Phys. Rev. B* **63**, 235323 (2001).
 - ¹⁵ Y. Wu, R. Fan, and P. Yang, *Nano Lett.* **2**, 83 (2002).
 - ¹⁶ M. S. Gudiksen, L. J. Lauhon, J. Wang, D. C. Smith, and C. M. Lieber, *Nature (London)* **415**, 617 (2002).
 - ¹⁷ M. T. Björk, B. J. Ohlsson, T. Sass, A. I. Persson, C. Thelander, M. H. Magnusson, K. Deppert,

- L. R. Wallenberg, and L. Samuelson, *Nano Lett.* **2**, 87 (2002).
- ¹⁸ R. Solanki, J. Huo, J. L. Freeouf, and B. Miner, *Appl. Phys. Lett.* **81**, 3864 (2002).
- ¹⁹ Z. H. Wu, M. Sun, X. Y. Mei, and H. E. Ruda, *Appl. Phys. Lett.* **85**, 657 (2004).
- ²⁰ L. C. Lew Yan Voon and M. Willatzen, *J. Appl. Phys.* **93**, 9997 (2003).
- ²¹ C. Galeriu, L. C. Lew Yan Voon, R. Melnik, M. Willatzen, *Comput. Phys. Comm.* **157**, 147 (2004).
- ²² L. C. Lew Yan Voon, B. Lassen, R. Melnik, and M. Willatzen, *J. Appl. Phys.* **96**, 4660 (2004).
- ²³ Yu-Ming Lin and M. S. Dresselhaus, *Phys. Rev. B* **68**, 075304 (2003).
- ²⁴ D. S. Citrin, *Phys. Rev. Lett.* **92**, 196803 (2004).
- ²⁵ Justino R. Madureira, Peter A. Schulz, Marcelo Z. Maialle, *Phys. Rev. B* **70**, 033309 (2004).
- ²⁶ S. Mizuno, *Phys. Rev. B* **71**, 085303 (2005).
- ²⁷ Enrique Diez, Rafael Gómez-Alcala, Francisco Domínguez-Adame, Angel Sánchez, and Gennady P. Berman, *Phys. Rev. B* **58**, 1146 (1998).

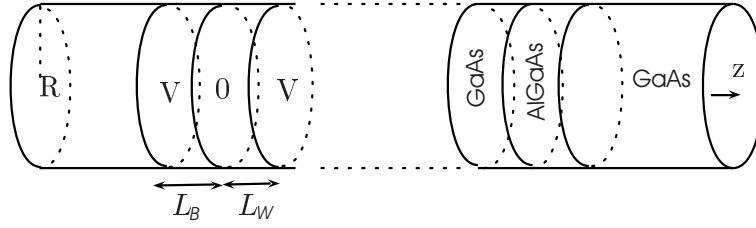


Fig. 1. Zhang et al.

FIG. 1: Nanowire superlattice with radius R , well width L_W , barrier width L_B , and potential energy V . The wire is capped on both sides by a thick cylindrical layer of GaAs.

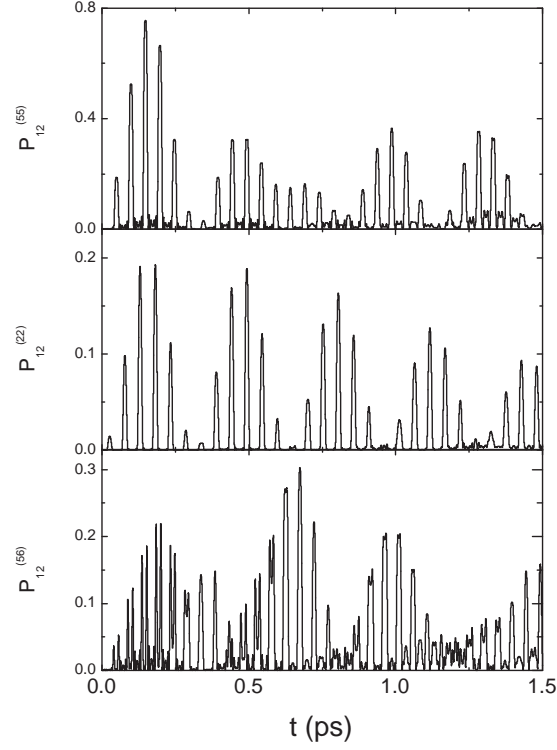


Fig. 2. Zhang et al.

FIG. 2: (a) Temporal evolution of $P_{12}^{(55)}(t)$ with $\omega_{ac} = (E_2^{(5)} - E_1^{(5)})/\hbar = 127$ THz. (b) Temporal evolution of $P_{12}^{(22)}(t)$ with $\omega_{ac} = (E_2^{(2)} - E_1^{(2)})/\hbar = 121$ THz. (c) Temporal evolution of $P_{12}^{(56)}(t)$ with $\omega_{ac} = (E_2^{(6)} - E_1^{(5)})/\hbar = 131$ THz. In all cases, $F = 50$ kV/cm and $R = 5$ nm.

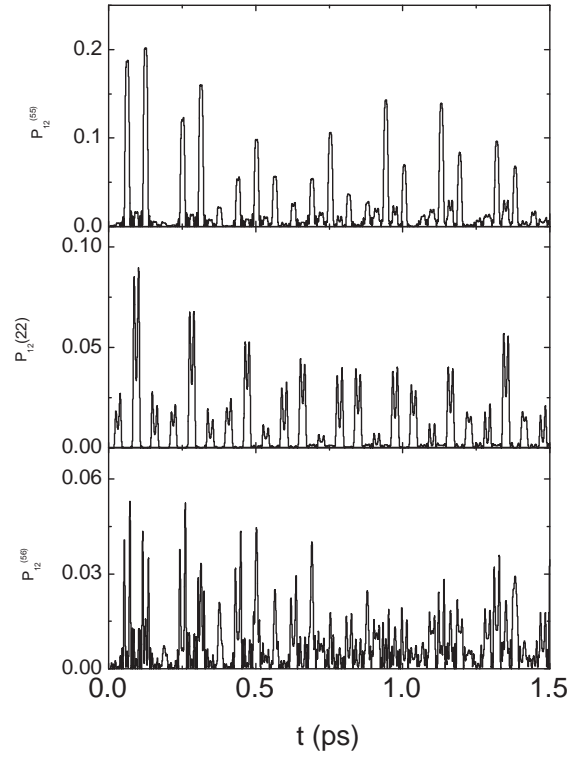


Fig. 3. Zhang et al.

FIG. 3: Temporal evolution of (a) $P_{12}^{(55)}(t)$, (b) $P_{12}^{(22)}(t)$, and (c) $P_{12}^{(56)}(t)$ with $F = 50$ kV/cm, $\omega_{ac} = 100$ THz, and $R = 5$ nm.

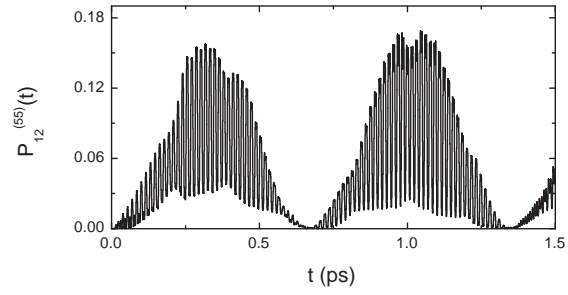


Fig. 4. Zhang et al.

FIG. 4: Temporal evolution of $P_{12}^{(55)}(t)$ with $\omega_{ac} = (E_2^{(5)} - E_1^{(5)})/\hbar = 127$ THz, $F = 50$ kV/cm, and $R = 1$ nm.